8. Dual-Wavelength Fiber Laser for 5G and Lidar Applications.

Hani J. Kbashi and Vishal Sharma

https://orcid.org/ 0000-0002-6343-248X

Contents

ABSTRACT

This chapter illustrates the generation of the millimeter-wave in the range of 10 GHz to 110 GHz using a tunable dual-wavelength erbium-doped fiber laser. It is also describes the utilization of these millimeter-waves as carrier frequencies for the transmission of 16-QAM with a data rate of 10 Gb/s over a Radio over fiber and free space optics links. The chapter also includes the utilization the millimeter-waves, that are generated in the designed dual-wavelength fiber laser, for estimating the target range and velocity of multiple radar cross-section defined automotive targets by developing a frequency-modulated continuous-wave photonics-based radar system in the presence of environmental fluctuations. We believe that the proposed dual-wavelength fiber laser described in this chapter will reveal the potential of realizing different microwave-photonic systems/networks, for instance, 5G/6G networks, self-driving vehicles, photonics-based radar systems, surveillance, and monitoring.

1.1 INTRODUCTION

Recently, fiber laser as a photonic source has attained revolutionary evolution in several fundamental technologies and applied sciences areas, including natural science studies, microwave-photonics, photonics-based telecommunication, optical spectroscopy, material processing, meteorology, sensing, surveillance & navigation, and medical-related applications (Kbashi 2018, Kolpakov 2016, Udem 2002, Yadav 2017, Fortier 2011, Tsai 2018, Dennis 1997, Sibbett 2012). Moreover, fiber lasers as a source of millimeter-wave/Terahertz (mmW/THz) wave generation (Kbashi 2021, Kbashi 2021) for telecommunication-related applications are gaining

popularity in the last few years through the interplay of gain/loss mechanisms along with linear and nonlinear effects. By maintaining these factors in a controlled manner, tuneable transmitters in mmW/THz band with high flexibility and stability are attainable. Additionally, a tuneable dual-wavelength fiber-laser (DWFL) for the generation of mmW is gaining considerable attraction nowadays due to its vast applications in the research and manufacturing sectors, including Autonomous vehicle-related industry and meteorology. Furthermore, compared to other various techniques (Gao 2012, Adany 2009, Morris 2012), the significant interest in dual-wavelength generation using a single fiber laser offers a high mutual coherence, common noise cancellation, compact size of a high-frequency signal source together with a simple and economical design along with high scalability to the state-of-the-art microwave-photonics networks. Also, due to low phase-noise and high phase-coherence, DWFL lasers have the potential for the realization/implementation of futuristic 5G/6G networks, for instance, radio over fiber (RoF) systems (Kbashi 2021), free-space optics (FSO) (Kbashi et al, 2021), hybrid microwave-optics systems (Zhu and Li, 2017), photonics-based Radar system (Sharma 2021), and Terahertz (THz) radiation-related applications (Hu 2018).

Alternatively, the state-of-the-art Autonomous Vehicles (AVs) demand high-resolution radar imaging to track multiple targets in complex traffic scenarios for all-weather situations. Subsequently, an mmW band (74 GHz-77 GHz) is preferred to achieve a high bandwidth of ≈ 4 GHz for the manufacturers. According to the range-resolution equation, $L_{res} = c/2B$, the broadened signals improve the radar resolution and reduce its size considerably [Ramasubramanian and Ramaiah, Zhang, Sharma, and Sergeyev]. Additionally, the environmental fluctuations become catastrophic in the urban- and industry-predominated zones due to dense

gasses, massive smoke, and airborne particles. It becomes difficult to retrieve the range-speed measurements unambiguously from the weak echoes. So, it becomes a challenging task to identify the mobile/immobile targets of different dimensions on the road accurately.

The enhanced radar resolution further augments the detection capability and can play a crucial role in poor visibility situations. Besides it, the current AVs are equipped with the driver assistance system (DAS), including the conventional microwave radar systems, three-dimensional cameras, and signal processing units. However, it offers a limited detection range with marginal resolutions at high power requirements [Sharma and Sergeyev]. Therefore, the light-based automotive radar system proves to be an attractive candidate for state-of-the-art surveillance, tracking, and navigation-like applications.

Alternatively, the high-power and phase-stable mmW generation in the preferable frequency band *(*74 GHz-77 GHz) using the traditional electronics-based techniques is a thought-provoking task. So, dual-wavelength fiber lasers have been designed efficiently in the last few years to realize self-driving and surveillance-related applications in this preferred band [Khattak 2018, Gao 2012, Adany 2009]. Moreover, DWFL-based mmW generation is free from using a microwave source, thus offering less complexity, low phase noise, and economical. However, the erbium-doped fiber-employed DWFL lasers experience mode-competition problems in the 1550 nm vicinity. Several expensive and complex demonstrations to manage this mode-competition issue have been established [Yan 2017, Zhou 2015, Khattak 2018, Lian 2017]. Subsequently, this chapter demonstrates an erbium-doped fiber-based tunable DWFL to generate mmW at 77 GHz in a simple configuration without using any additional high-quality microwave source. These generated mmW waves are utilized to develop a linear photonics-based radar system and are investigated under

severe atmospheric perceptions. The designed DWFL is tunable over 0.1-0.9 nm, corresponding to the mmW frequency range of ~12.3-110 GHz with a tunable step of ~10 GHz. To validate the proposed fiber-laser in 5G-related applications, successful transmission of 16-QAM modulated signals at a data rate of 10 Gb/s over the RoF and FSO link is demonstrated. Further, the proposed laser is developed to realize an automotive photonics-based radar system in successive sections.

1.2 DUAL-WAVELENGTH FIBER LASER EXPERIMENTAL SETUP AND CHARACTERIZATION

The experimentally simple and compact DWFL configuration is illustrated in Fig. 9.1(a). A nonlinear polarization rotation (NPR) ring-cavity is formed consisting of one-meter Er-doped fiber, 10 m of polarization maintaining fiber, and 9.1 m of single-mode slandered telecommunication fiber (SMF) making an overall cavity length of 20.1m. The high concentration erbium-doped active fiber (*Liekki Er80-8/125*) is pumped using a 980-nm laser diode via a wavelength-division-multiplexer (*WDM-980/1550 nm*). While the two polarization controllers (PCs) together with the polarization-independent optical isolator (ISO) achieve a phase-stable NPR lasing action and adjusting/maintaining the laser net cavity-birefringence; ISO also ensures a unidirectional circulation inside the cavity. An accurate optical filtering inside the laser cavity, over a wide spectral band to attain a uniform channel-spacing, is attained by incorporating a 10-m high birefringence (HiBi) fiber (NA = 0.125; Core/Cladding = 8.5/125 μm). It helps in generating high phase-stable dual-wavelengths by stabilizing the state of polarization. A 90:10 fused fiber output coupler is incorporated to feedback about 90% of the signal power inside the cavity and

about 10% of the signal power is used for the spectral and temporal study using a fast 17 GHz photodetector (InGaAsUDP-15-IR-2_FC) linked to a 2.5 GHz sampling oscilloscope *(Tektronix DPO7254)*. A polarimeter (Thorlabs IPM5300) of 1 μs resolution in a time-interval ≈ 1 ms (25–40000 roundtrips) is used to compute the normalized Stokes parameters (S_1, S_2, S_3), and degree of polarization (*DOP*). An optical spectrum analyzer (Yokogawa AQ6317B) of maximum resolution ≈ 20 pm, and a radio frequency spectrum analyzer observe the optical and the RF spectrum respectively. Fig. 9.1(b) shows the measured output power from 10% of the output coupler vs pump power showing a very low threshold of laser ≈ 20mW and a high output power ≈ 80 mW with a power efficiency of ≈ 35%.

FIGURE 9.1

Fig. 9.1. (a) The experimental setup of the proposed switchable dual-wavelength fiber laser: Er80: high concentration erbium-doped fiber, $PC_{1,2}$: polarization controllers, WDM: a wavelength division multiplexing coupler, ISO: an optical isolator, HiBi: high birefringence fiber; (b) the measured output power from the 10% of the output coupler vs pump power [Kbashi 2021]. (Adapted from H. Kbashi, V. Sharma, S. Sergeyev. 2021. "Phase-stable millimeter-wave generation using switchable dual-wavelength fiber laser." Optics and Lasers in Engineering, 137 106390).

By proper adjustment of the pump power initially at 20mW and the net birefringence of the cavity using the two PCs, a dual-wavelength lasing is attained with a wavelength spacing of 0.1 nm and then, it is perfectly tuned from 0.1-0.89 nm sequentially, as shown in Fig. 9.2(a), conforming to beat frequency ≈ 12.5 GHz -110 GHz (mmW) as shown in Fig. 9.2(b). The observations show that

initially, the dual-wavelength peaks at 0.1 nm are located at 1560.0 nm and 1560.1 nm with a narrow linewidth of 0.125 nm and 0.13 nm, respectively. However, the laser peaks at 0.89 nm are observed at 1559.54 nm and 1560.43 nm with a narrow linewidth of 0.12 nm and 0.1 nm, respectively.

FIGURE 9.2

Fig. 9.2 (b) tunable dual-wavelength emission spacing at (1) 0.1 nm, (2) 0.46 nm, (3) 0.63 nm, (4) 0.7 nm, and (5) 0.89 nm; (c) the corresponding mmW from 12.5 GHz to 110 GHz [Kbashi 2021].

(Adapted from H. Kbashi, V. Sharma, S. Sergeyev. 2021. "Phase-stable millimeter-wave generation using switchable dual-wavelength fiber laser." Optics and Lasers in Engineering, 137 106390.

Further, the phase-stability of the generated dual-wavelength peaks at 1559.5 nm and 1560.35 with a wavelength spacing of 0.85 nm are observed by analyzing the output spectra for 60 minutes with a scanning-interval of 10 minutes, as illustrated in Fig. 9.3(a). Fig. 9.3(a) shows phase-stable spectra, free from any wavelength shift, during the observation period with an optical signal-to-noise ratio (≈ 40 dB). Further, a low power fluctuation of 0.32 dB and wavelength peak-fluctuation ≈ 0.03 nm at 56 GHz are also measured over the observation period (Kbashi 2021). A phase-stable dual-wavelength operation may attain due to maintaining the state of polarization by incorporating the HiBi fiber and it may efficiently overpower the mode competition of the homogenous line-

broadening and cross-gain saturation in the Er-doped fiber. Moreover, the PCs with HiBi may provide a wavelength-dependent polarization rotation and fluctuates in the state of the polarization (SOPs) across the multiple wavelengths. Together it may also support attaining an optimal amplification at low pump power by managing the SOPs and providing a linearly polarized output that further leads to a phase-stable tunable laser.

The beat length (L_b) and the difference between the two orthogonal polarization refractive indices as a function of the dual-wavelength spacing are calculated using equations 1.1 and 1.2. The results are shown in Fig. 9.3(b). The beating length is tuned from ≈1.3 mm to ≈12 mm by maintaining the total cavity birefringence via controlled adjustment of the PCs. It leads to an increase in the free spectral range of the HiBi fiber and measures the difference between the two orthogonal polarization refractive indices in the range of minima to maxima as 1.35×10^{-4} to 1.2×10^{-3} in this experiment.

$$L_b = \frac{\Delta\lambda}{\lambda}.L \tag{1.1}$$

$$\Delta n_{eff} = \frac{\lambda}{L_b} \tag{1.2}$$

Where L_b is the polarization beating length, $\Delta\lambda$ is the dual-wavelength separation, λ is the central wavelength, L is the laser cavity length and Δn_{eff} is the polarization refractive indices.

FIGURE 9.3

Fig. 9.3. (a) Stability spectra of the DWFL-based generation with wavelength-spacing of 0.85 nm; (b) the beat-length and the two orthogonal polarization refractive-indices variation as a function

of different dual-wavelength spacing. (Adapted from H. Kbashi, V. Sharma, S. Sergeyev. 2021. "Phase-stable millimeter-wave generation using switchable dual-wavelength fiber laser." Optics and Lasers in Engineering, 137 106390).

The SOP dynamics of the DWFL have been characterized using a polarimeter by measuring the normalized Stokes parameters, i.e. S_1, S_2, S_3, and the degree of polarization (DOP). The polarimeter has a resolution of 1 μs and a measurement interval of 1 ms (25 – 25000 round trips) and detects the normalized s_1, s_2, s_3 and the DOP which are to the output powers of two linearly cross-polarized SOPs, $|u|^2$ and $|v|^2$, and the phase difference between them $\triangle\phi$:

$$S_0 = |u|^2 + |v|^2,\ S_1 = |u|^2 - |v|^2,\ S_2 = 2|u||v|\cos\Delta\varphi,\ S_3 = 2|u||v|\sin\Delta\varphi,$$

$$s_i = \frac{S_i}{\sqrt{S_1^2+S_2^2+S_3^2}},\quad DOP = \frac{\sqrt{S_1^2+S_2^2+S_3^2}}{S_0}, (i = 1,2,3) \qquad (1.3)$$

Fig. 4 illustrates a stable polarization operation for most of the observed dual-wavelength regimes (as for 0.1 nm-0.48 nm) in the Poincare sphere with the axis defined by the three Stokes parameters. These stable and slow polarization dynamics indicate a high coherent coupling between the two orthogonal polarization which leads to produc a single-pulse (mode-locked) regime as in 0.1 nm, 0.29 nm, and 0.48 nm due to the synchronization of two orthogonal SOPs. Furthermore, the laser system starts desynchronizing the two orthogonal SOPs at 0.7 nm while attaining a complex chaotic regime at 0.89 nm as shown in Fig. 9.4(a). This indicates an incoherent coupling between the two orthogonal polarizations as the DOP is decreased to < 40% (Fig. 9.4(b)). Moreover, this synchronization and coupling behavior can be described via the vector resonance multimode instability [Sergeyev S. V].

FIGURE 9.4

Fig. 9.4. (a) the SOP; (b) DOP of the switchable dual-wavelength fiber laser-based generation at different wavelength spacing, 1 - 0.1 nm; 2 - 0.29 nm; 3 - 0.48 nm; 4 - 0.7 nm; and 5 – 0.89 nm. (Adapted from H. Kbashi, V. Sharma, S. Sergeyev. 2021. "Phase-stable millimeter-wave generation using switchable dual-wavelength fiber laser." Optics and Lasers in Engineering, 137 106390).

1.3 DWFL FOR MILLIMETER WAVES (5G) TRANSMISSION APPLICATIONS.

1.3.1 Transmission of mmW waves over Radio-over-Fiber (ROF) link

The proposed tunable DWFL designed experimentally in the previous section has enormous opportunities in futuristic 5G/6G transmission systems including RoF, FSO transmission systems, and automotive LiDAR systems. This section deals with the implementation of orthogonal frequency-division multiplexing (OFDM) incorporated RoF transmission system to transmit a data rate of 10 Gb/s (16-QAM signals) over four different RF carrier frequencies, i.e. 56.7, 77.6, 86.2, and 110 GHz, which are generated by using the tunable DWFL laser as shown in Fig. 9.5. The OFDM-RoF system is demonstrated by co-simulating the *Optisystem*^{TM} photonic module and *MATLAB*^{TM} software. The antenna module is designed using the *MATLAB*^{TM} software which is integrated with *Optisystem*^{TM} using *MATLAB.dll* files. By co-simulating both software-based modeled sub-systems, the tunable DWFL-based mmW waves are generated and then transmitted over the OFDM-RoF link. Fig. 9.5 shows the simulation setup for transmitting the proposed laser-based generated RF signals over the RoF link.

The dual-wavelength optical signals, for instance, 0.46 nm (~ 56.7 GHz) are separated using DWDM (1:2 splitter) into two wavelengths (1558.94 nm and 1559.40 nm). In the first arm of the splitter, the OFDM modulated data signals that are generated employing a 16-QAM digital modulation via a local oscillator (LO) are optically modulated over the optical frequency carrier of 1559.40 nm using a Mach Zehnder modulator (MZM). A suitable optical bandpass filter (OBPF) has been used with a center wavelength of 1559.40 nm to filter out the high sideband and only obtain the lower sideband of the QAM signals i.e. LSB-QAM. This LSB-QAM signal is applied to another DWDM (2:1 combiner) to combine with the unmodulated output signal in the second arm of DWDM. The obtained LSB-QAM modulated signals at the output of the combiner are propagated over SMF fiber (20 Km) and then intensified using a low-noise EDFA amplifier to restore the optical power budget. These modulated OFDM signals are mixed with the unmodulated carrier signals at the radio access unit (RAU) in a PIN photo-detector with a responsivity of 0.8 A/W to generate the required mmW signals, which are further then transmitted over a wireless link using a transmitting antenna (Gain ≈ 25 dBi). At the receiver side, the original information is retrieved by the demodulation process using the local oscillator (LO) and a microwave demodulator.

However, an additive white Gaussian noise (AWGN) wireless channel is designed using *MATLAB*^{TM} and is integrated with the *Optisystem*^{TM} photonic-module to realize the RoF system. In the 55-60 GHz frequency band, the atmospheric factors like absorption by atmospheric gasses, water vapor density, and other atmospheric constituents offer a significant signal-fading under dry and standard atmospheric situations [Zibar 2011]. It causes a weak signal reception at the radio unit (*RU*) and leads to a short transmission range. Therefore, due to the high attenuation of signals

in this frequency band with geometric losses, it is essential to restore the required signal power by applying a suitable amplification. Therefore, the received signals are amplified at the RU unit using a low-noise amplifier (LNA) of 17 dB in the demonstrated mmW band (56 GHz- 110 GHz) with a noise figure of ≈ 5 dB [Bessemoulin 2011, Zibar 2011] after propagating through the wireless link. These amplified signals are applied to a band pass filter (BPF) after OFDM-demodulation to retrieve the transmitted data signals.

FIGURE 9.5

Fig. 9.5. Simulation setup of Tunable DWFL-driven RoF transmission system.

(Adapted from H. Kbashi, V. Sharma, S. Sergeyev. 2021. "Dual-Wavelength Fiber-Laser-based Transmission of Millimeter waves for 5G-supported Radio-over-Fiber (RoF) links." Optical Fiber Technology Vol. 65, 102588).

The performance evaluation of the DWFL derived OFDM-RoF system is computed in terms of eye diagrams, bit-error-rate versus signal-to-noise ratio, and constellation diagram as shown in Figs. 6-8, which confirmed the successful transmission of OFDM data signals centered at the generated mmW frequencies (56.7, 77.6, 86.2, and 110 GHz) analogous to the dual-wavelength separation of the proposed dual-wavelength laser. Fig. 9.6 shows the eye diagram estimation of the transmitted signals over SSMF of 20 Km at varied wavelength spacing at the radio access unit after photo-detection. Furthermore, the BER estimation as a function of wireless link length and SNR ratio is carried-out to achieve the threshold BER of 10^{-3}. The outcomes reveal that as the transmission occurs at a higher frequency of the millimeter-wave band, the SNR penalty increases

to obtain the threshold BER (10^{-3}). As per the atmospheric impact on the transmission of mmW signals beyond the mid-boundary of the EHF frequency band of the 5G frequency spectrum [Zibar 2011, Bessemoulin 2005], the link- length reduces along with the augmentation of power penalty to achieve the threshold BER as shown in Fig. 9.7 and Fig. 9.8. An SNR penalty of ≈ 25 dB and ≈ 34 dB is required to attain the BER of 10^{-3} at 55.6 GHz over a wireless link of 10 m and 50 m, respectively. For the successful transmission at 110 GHz, a power penalty of ≈ 35 dB and ≈ 45 dB is required over the demonstrated link lengths due to high fading in this frequency band. Thus, this work shows the feasibility of using the proposed laser for realizing the RoF transmission systems over a wide span of mmW band with a possibility of attaining an effective data rate of ≈ 100 Gbps over a wireless link up to ≈ 10 m using the existing state-of-the-art 75-110 GHz antenna technology capable of providing a combined antenna gain of ≥ 48 dBi. Moreover, the spatial diversity and beamforming techniques may play a significant role in achieving high transmission data rates in non-LOS environments at minimal power requirements.

FIGURE 9.6

Fig. 9.6. Eye diagram estimation over fiber link of 20 Km at wavelength spacing of (a) 0.46 nm (b) 0.63 nm (c) 0.70 nm, and (d) 0.89 nm. (Adapted from H. Kbashi, V. Sharma, S. Sergeyev. 2021. "Dual-Wavelength Fiber-Laser-based Transmission of Millimeter waves for 5G-supported Radio-over-Fiber (RoF) links." Optical Fiber Technology Vol. 65, 102588).

FIGURE 9.7

Fig. 9.7. BER measurements versus SNR penalty at varied mmW signals over the wireless link of

(a) 10 meter, and (b) 50 meter. (Adapted from H. Kbashi, V. Sharma, S. Sergeyev. 2021. "Dual-Wavelength Fiber-Laser-based Transmission of Millimeter waves for 5G-supported Radio-over-Fiber (RoF) links." Optical Fiber Technology Vol. 65, 102588).

FIGURE 9.8

Fig. 9.8. Constellation diagrams over wireless link of 10 meter at (a) 56.7 GHz (@ SNR = 25 dB, (b) 77.6 GHz (@ SNR = 29 dB, (c) 86.2 GHz (@ SNR = 31.5 dB, and (b) 110 GHz @ SNR = 35 dB. (Adapted from H. Kbashi, V. Sharma, S. Sergeyev. 2021. "Dual-Wavelength Fiber-Laser-based Transmission of Millimeter waves for 5G-supported Radio-over-Fiber (RoF) links." Optical Fiber Technology Vol. 65, 102588).

1.3.2 TRANSMISSION OF MMW WAVES OVER FREE-SPACE OPTICS (FSO) LINK

We have also designed the optical communication system to transmit a data rate of 10 Gb/s (16-QAM signals) over FSO using four different carrier frequencies (56.7, 77.6, 86.2, and 110 GHz) that are generated by the DWFL. The schematic diagram for carrying out the transmission of 16-QAM signals over the FSO link is shown in Fig. 9.9. This high data rate has been transmitted over the FSO link using Optisystem photonic module to validate the potential of the proposed laser. The dual-wavelength optical signals, for instance, 0.46 nm (~ 56.7 GHz) are separated using DWDM (1:2 splitter) into two wavelengths (1558.94 nm and 1559.40 nm). In the first arm of the splitter, the 16-QAM are optically modulated over the optical frequency carrier of 1559.40 nm using a MZM. A suitable optical BPF has been used with a center wavelength of 1559.40 nm to

filter out the high sideband and only obtain the lower sideband of the QAM signals i.e. LSB-QAM. This LSB-QAM signal is applied to another DWDM (2:1 combiner) to combine with the unmodulated output signal in the second arm of DWDM. The obtained LSB-QAM modulated signals at the output of the combiner are transmitted over 20 Km of SMF and then to the FSO wireless channel of 500 m. The LSB-QAM signals are amplified before transmitting through the FSO link by using low-noise EDFA (gain=17dB, NF=5dB) to restore the optical power budget. The proposed transmitter and receiver telescopic lens have an aperture diameter of 5 cm and 15 cm respectively with a beam divergence of 2 mrad. The FSO link attenuation of 21 dB/Km is considered with fiber-telescope coupling losses equal to 1 dB; geometrical losses equal to 2 dB; mispointing equal to 5 dB. At the receiver side, the received 16-QAM is detected using a PIN photodetector with a responsivity of 0.8 A/W. Due to the attenuating wireless link, an electrical amplifier is used to amplify the received weak signal. To obtain the baseband signal, the received electrical signals are passed out of a low pass filter (LPF) and are demodulated using a QAM demodulator.

FIGURE 9.9

Fig. 9.9: Schematic diagram of the 5G transmission over FSO link using erbium-doped DWFL.

The system transmission performances are considered by measuring the SNR and BER at different FSO link-length for up to 500 meters. From the obtained results as illustrated in Fig. 9.10(a), it has been shown that the 16 QAM data are transmitted effectively through the FSO link for more than 500 m, ≈350 m, ≈275 m, and 200 m using the carrier frequencies of 56.7 GHz, 77.6 GHz, 86.2

GHz, and 105 GHz respectively. Additionally, BER consideration as a function of the FSO link is also carried out as shown in Fig. 9.10(b), which reveals that the achievable transmission link reduces to obtain the acceptable BER of 10^{-3} target at a higher mmWaves frequencies. These results are computed based on the SNR threshold value of 15 dB for all four carrier frequencies showing clearly that the 16-QAM data signals of 10 Gb/s are transmitted successfully.

FIGURE 9.10

Fig. 9.10. (a) SNR and (b) BER measurements of the 5G transmission driven by DWFL.

1.4 DWFL FOR LIDAR APPLICATIONS

1.4.1 Experimental Results and Discussion

The designed and demonstrated DWFL [Kbashi et. al. 2021] have been utilized to develop a linear frequency-modulated continuous-wave (FMCW) photonics-based radar system to compute the range and speed of several vehicles unambiguously in a modeled traffic scenario via co-simulation of *MATLAB*^{TM} and *OptiSystem*^{TM} software. After a precise adjustment of the polarization controllers in the DWFL setup, a dual-wavelength at λ_1=1559.50 nm and λ_2=1560.125 nm is attained and generated corresponding mmW waves of 77 GHz as shown in the RF spectra in Fig. 9.11.

FIGURE 9.11

Fig. 9.11: RF signal at 77 GHz after proper tuning of the laser at wavelength spacing of 0.625 nm.

Fig. 9.12 depicts the basic idea of a DWFL-driven linear FMCW photonics-based radar system that employs the proposed laser to utilize as an RF carrier and a light-based carrier-source simultaneously. A linear frequency-modulated signal (LFM) is generated using the proposed laser output (at Port 1) tuned to 77 GHz and a sawtooth pulse generator. The generated LFM radar signals are further optical modulated over the laser output (at Port 2) via an external dual-electrode MZM after passing through a tunable bandpass filter centered at 1559.5 nm. The LFM signal is fed directly to the first arm of the modulator. It is applied to the second arm of the modulator through a phase-shifter. The unwanted higher-order sidebands are suppressed by adjusting the bias voltages of the external modulator [Sharma 2021, Sharma 2020].

This optical treatment extends the spectral width of the LFM radar signals which helps in improving the radar resolutions. These spectrally broadened signals are transmitted towards the target objects using an antenna module after photo-detection through a narrowband line-of-sight (LOS) channel. The channel is modeled as per ITU-R P.838-3 and ITU-R P.840-6 recommendations [ITU-R P.838-*3* and ITU-R P.840-6], including the water vapor-density, dry-air pressure, liquid water-density, and rainfall rate, to compute the impact of weather perceptions as these degrade the radar signals significantly at mmW frequencies. The channel is developed using the phased-array tool of *MATLAB*^{TM} and is further co-simulated with the well-known photonics-based simulation tool, i.e. *OptiSystem*^{TM} to investigate the DWFL-driven photonics-based radar.

FIGURE 9.12

Fig 9.12. Schematic diagram of DWFL-driven LFMCW-PHRAD system.

A traffic scenario is also developed, including large-and small-sized automotive mobile targets, i.e. cars, trucks, motorbikes, bicycles, and pedestrians traveling at different relative velocities (1.11 m/s, 5.55 m/s, 8.33 m/s, 20.83 m/s, and 26.38 m/s respectively) at diverse target-ranges (490 m, 400 m, 350 m, 300 m, and 250 m respectively) upfront of the observatory vehicle moving at 100 km/hr assuming all the target vehicles moving towards it. All the target objects are defined by their associated radar cross-section (RCS*)* at 77 GHz as per [Yamada 2021, Sharma 2021]. A down-conversion of the reflected echoes with the instantaneous transmitted signal is carried out to measure the beat frequency. A down-conversion of the reflected echoes with the instantaneous transmitted signal is carried out to measure the beat frequency and thus, the detection range. The received de-chirp signals for 128 sweeps are stored in a buffer to retrieve the Doppler shift. Then, a two-dimensional fast Fourier transformation with the Hanning window is applied to measure the range and speed concurrently of the illuminated targets corresponding to the retrieved beat frequency and Doppler-shift information at a minimal false alarm rate [Sharma 2021, Sharma 2020].

Under a clear-weather scenario shown in Fig. 9.13, the LOS channel is modeled with dry air pressure = 101, water-vapour density = 0, liquid water-density = 0, and rainfall rate = 0 mm/hr. The beat-frequency is measured as 267.19 MHz, 245.51 MHz, 218.55 MHz, 136.52 MHz, and 191.02 MHz with signal-intensity of -103.83 dBm/Hz, -111.39 dBm/Hz, -112.512 dBm/Hz, -122.5 dBm/Hz, and -112.06 dBm/Hz for truck, car, bike, bicycle, and pedestrian respectively. For severe weather situations, including the influence of heavy rain and heavy fog, the LOS channel is modeled with a liquid water density = 7.5, liquid water density = 2.5, and rainfall rate = 50 mm/hr [Sharma 2021, Sharma 2020, Yamada 2001]. The impact of smoke, atmospheric gasses, and dust

particles are not considered for all the considered scenarios in this work. For the severe weather scenario shown in Fig. 9.14, the beat-frequency is measured with the signal intensity of -124.95 dBm/Hz, -1130.66 dBm/Hz, -126.68 dBm/Hz, -133.38 dBm/Hz, and -127.15 dBm/Hz for the targets under observations in the same order of the clear-weather scenario. The measured beat frequency of the demonstrated DWFL-driven LFMCW-PHRAD matches the theoretical measurements with a marginal frequency error of a few kHz. The attained outcomes reveal that heavy fog and rain have a substantial influence on the detection range and the echo strength. A difference in signal fading of 21.12 dBm/Hz, 19.27 dBm/Hz, 14.17 dBm/Hz, 10.88 dBm/Hz, and 15.09 dBm/Hz is recorded for truck, car, bike, bicycle, and pedestrians respectively in the presence of fog + cloud + rain scenario contrast to the clear-weather scenario. It is also observed that the reduction in signal strength of the received reflected radar signals varies following the target range and the associated RCS of the illuminated targets. The other measurements of the LFMCW-PHRAD system, like SNR, signal-to-noise and distortion ratio (SINAD), and spurious-free dynamic range (SFDR), are recorded as 43 dBm, 43 dBc, and 55 dBc, respectively. The recorded observations validate the ability of the demonstrated laser to realize smart transportation systems and diverse 5G-supported microwave-photonics systems as it generates stable millimeter waves over a wider band (12 GHz-110 GHz).

FIGURE 9.13

Fig 9.13. Measurements in terms of (a) PSD, and (b) Doppler mapping under clear-weather scenario for DWFL-driven LFMCW-PHRAD system.

FIGURE 9.14

Fig 9.14. Measurements in terms of (a) PSD, and (b) Doppler mapping under the collective influence of environmental factors.

CHAPTER CONCLUSIONS.

In this chapter, we demonstrate the tunable dual-wavelength erbium-doped fiber laser to generate millimeter-wave signals over a wide range of 10 GHz to 110 GHz using an erbium-doped and high birefringence fibers in NPR ring configuration. This DWFL source has been successfully realized for transmission of16-QAM with the data rate of 10 Gb/s over RoF and FSO links with an acceptable SNR and BER for all four different generated mm-waves carrier frequencies (56.7 GHz, 77.6 GHz, 86.2 GHz, 110 GHz).

We have also utilized the DWFL laser for estimating the target range and velocity of multiple RCS-defined automotive targets by developing an LFMCW-PHRAD in the presence of environmental fluctuations via *MATLAB*^{TM} and *OptiSystem*^{TM} software. Due to attaining a uniform wavelength spacing, along with low phase noise, the established DWFL-driven LFMCW-PHRAD system can provide phase-stable and spectrally-broadened optical-modulated radar signals for achieving high imaging resolutions with high accuracy. As the demonstrated photonics-based radar system is established in a simulative environment using the experimentally designed DWFL laser, an end-to-end fully experimental system may be implemented in the future to realize futuristic 5G-supported smart transportation systems/networks, tunable multiband photonics-based radar systems and automotive photonics radar services using the demonstrated economical DWFL system.

REFERENCES

Adany P., Allen C., and Hui R. 2009. "Chirped lidar using simplified homodyne detection." *Journal of Lightwave technology,* vol. 27, pp. 3351-3357.

Bessemoulin A. et al. 2005. "High gain 110-GHz low noise amplifier MMICs using 120 nm metamorphic HEMTs and coplanar waveguides." *European Gallium Arsenide and Other Semiconductor Application Symposium, GAAS,* Paris, France, pp. 77-80.

Dennis M. L., Putnam M. A., Kang J. U., Tsai T.-E., Duling I. N., and Friebele E. J. 1997. "Grating sensor array demodulation by use of a passively mode-locked fiber laser." *Optics Letters*, vol. 22, pp. 1362-1364.

Fortier T. M., Kirchner M. S., Quinlan F., Taylor J., Bergquist J., Rosenband T., et al. 2011. "Generation of ultrastable microwaves via optical frequency division." *Nature Photonics*, vol. 5, pp. 425-429.

Gao, O'Sullivan M., Hui, R. 2012. "Complex-optical-field Lidar system for range and vector velocity measurement." *Optics Express,* vol. 20, pp. 25867-25875.

Hu G., Mizuguchi T., Oe R., Nitta K., Zhao X., Minamikawa T., Li T., Zheng Zh. and Yasui T. 2018. "Dual terahertz comb spectroscopy with a single free-running fiber laser." *Scientific Reports,* 8:11155.

ITU-R P.838-3, "Specific attenuation model for rain for use in prediction methods," (2005).

ITU-R P.840-6, "Attenuation due to clouds and fog", (2013).

Lian Y. et. al. 2017. "Switchable multi-wavelength fiber laser using erbium-doped twin-core fiber and nonlinear polarization rotation." *Laser Phys. Lett*., 14, 055101.

Kbashi H. J., Sergeyev S. V. , Mou Ch., Garcia A. M., Al Araimi M., Rozhin A., Kolpakov S., Kalashnikov V. 2018. "Bright-Dark Rogue Waves." *Annalen der Physik*, 530, 1700362.

Kbashi H. J., Sharma V., Sergeyev S. 2021. "Phase-stable millimeter-wave generation using switchable dual-wavelength fiber laser." Optics and Lasers in Engineering, 137 106390.

Kbashi H. J., Sharma V., Sergeyev S. 2021. "Dual-Wavelength Fiber-Laser-based Transmission of Millimeter waves for 5G-supported Radio-over-Fiber (RoF) links." *Optical Fiber Technology*, 65, 2021, 102588.

Kbashi H. J., Sharma V., Sergeyev S. 2021. "Transmission of 5G using Tunable Dual-Wavelength Fiber Laser." *2021 Conference on Lasers and Electro-Optics Europe (CLEO), Microwave Photonics (ci_3)***,** Munich Germany, 21–25 June 2021, ISBN: 978-1-6654-1876-8.

Khattak, G. Tatel, and Wei L. 2018. "Tunable and Switchable EDF Laser Using a Multimode-Fiber Based Filter." *App. Sci*, 8, 1135.

Kolpakov SA, Kbashi H. J., Sergeyev S. V. 2016. "Slow optical rogue waves in a unidirectional fiber laser" *2016 Conference on Lasers and Electro-Optics (CLEO),* San Jose, California United States, 5–10 June 2016, ISBN: 978-1-943580-11-8 (2016): Science and Innovations, JW2A. 56.

Morris O. J, Wilcox K.G, Head C R., Turnbull A. P., Mosley P. J., Quarterman A. H., Kbashi H. J., Farrer I., Beere H. E., Ritchie D. A., Troppe A. C. 2012. "A wavelength tunable 2-ps pulse VECSEL, " *2012 Proc. SPIE 8242, Vertical External Cavity Surface Emitting Lasers (VECSELs) II, 824212, (14 February 2012),* San Francisco, California, United States; https://doi.org/10.1117/12.908337.

Ramasubramanian K., and Ramaiah, K. 2018. "Moving from legacy 24 GHz to state-of-the-Art 77-GHz Radar. "*ATZ Elekt.World,* 13, 46-49.

Sergeyev S. V., Kbashi H., Tarasov N., Loiko, Yu and Kolpakov S. A. 2017. "Vector-Resonance-Multimode Instability." *Phys Rev Lett*, 118, 033904.

Sharma V., Kbashi H. J., Sergeyev S. 2021. "MIMO-employed coherent photonic-radar (MIMO-Co-PHRAD) for detection and ranging." *Wireless Networks, Springer Nature,* vol 27, pp.2549–2558.

Sharma, V, Sergeyev, S, Kumar, L, Kbashi, Hani. 2020. "Range-speed mapping and target-classification measurements of automotive targets using photonic radar", *Optical and Quantum Electronics,* 52 (438) pp.3-18.

Sharma. V, and Sergeyev. S. 2020. "Range detection assessment of photonic-radar under adverse weather perceptions.", *Optics Comm,* 472.

Sharma, V and Kumar, L 2020. "Photonic-radar based Multiple-Target Tracking under complex traffic-environments", IEEE Access, (2020).

Sibbett W., Lagatsky A. A. and Brown C. T. A. 2012. "The development and application of femtosecond laser systems,*" Optics Express,* vol. 20, pp. 6989-7001.

Tsai Ch. T., Li Ch., Lin Ch., Ch. T. L. and Lin G., "Long-reach 60-GHz MMWoF link with free-running laser diodes beating," Scientific Reports, 8:13711, (2018).

Udem T., Holzwarth R. and Hansch T. W. 2002. "Optical frequency metrology." *Nature*, vol. 416, pp. 233-237.

Yadav A., Kbash H. J., Kolpakov S., Gordon N., Zhou K., and Rafailov E. U. 2017. "Stealth dicing of sapphire wafers with near infra-red femtosecond pulses." *Applied Physics A*, vol. 123, p. 369.

Yamada N. 2001. "Three-dimensional high-resolution measurement of radar cross section for car in 76 GHz band." *R&D review of Toyota Central R&D Labs*., 36 (2).

Yan N. et.al. 2017. "Tunable dual-wavelength fibre-laser with unique-gain system-based on in-fibre acousto-optic mach–zehnder interferometer." *Optics Express*, 25(22), 27609.

Zhang F. et. al. 2017. "Photonics-based real-time ultra-high-range-resolution radar with broadband signal generation and processing," *Sci. Rep.*, 7 (1), 1-8.

Zhou J. et.al. 2015. "Dual-wavelength single-longitudinal-mode fibre laser with switchable wavelength spacing based on a graphene saturable absorber." *Photonics Research*, 3(2), A21-A24.

Zhu D.-Q. and Li P.-B. 2017. "Preparation of entangled states of microwave photons in a hybrid system via the electro-optic effect." *Optics Express*, 25 (23).

Zibar D., Caballero A., Yu X., Pang X., Dogadaev A. K. and Monroy I. T. 2011. "Hybrid optical fibre-wireless links at the 75–110 GHz band supporting 100 Gbps transmission capacities." *2011 International Topical Meeting on Microwave Photonics jointly held with the 2011 Asia-Pacific Microwave Photonics Conference*, Singapore, 2011, pp. 445-449, doi: 10.1109/MWP.2011.6088767.

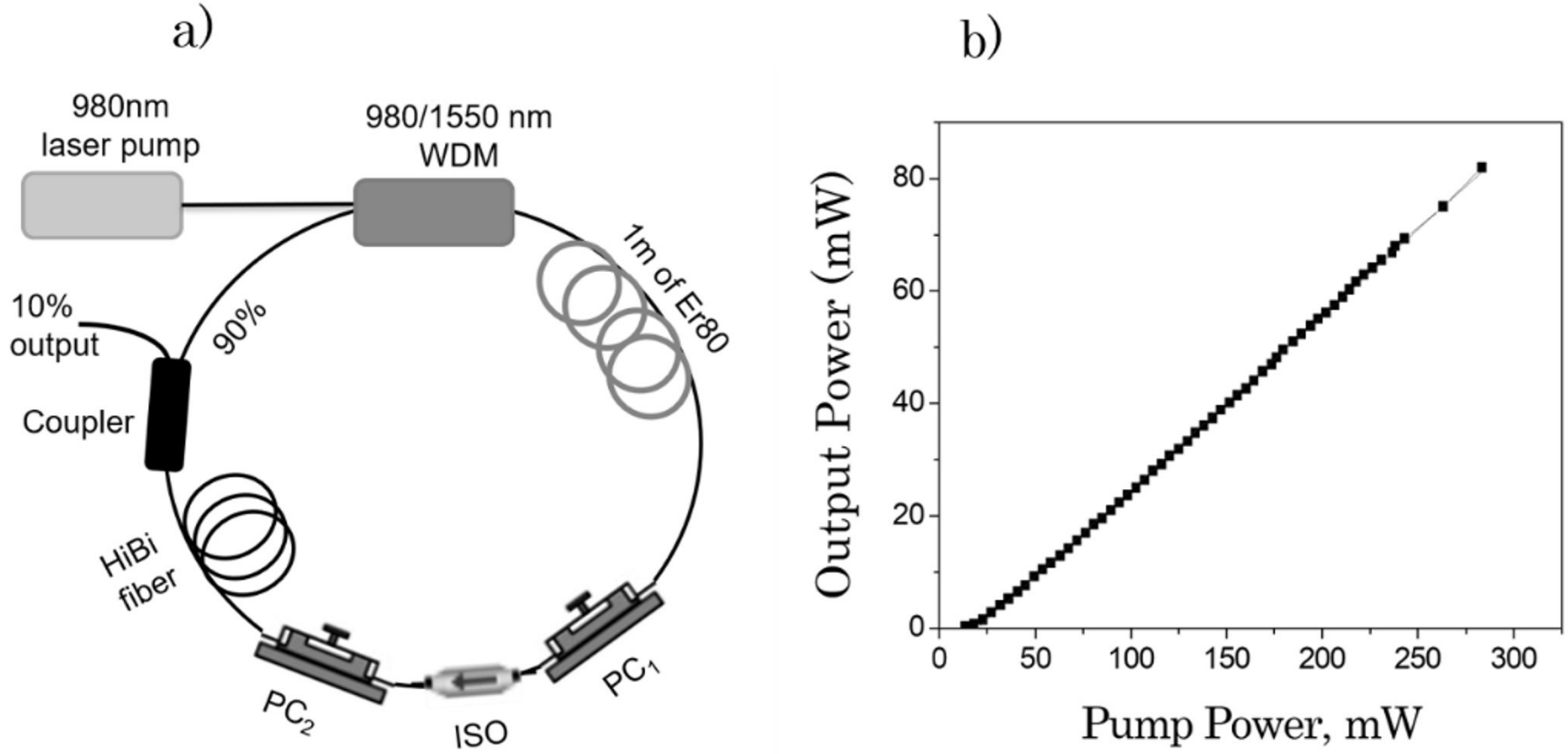
a)
980nm
laser pump
980/1550 nm
WDM
1m of Er80
10%
output
90%
Coupler
HiBi
fiber
PC2
ISO
PC1
b)
Output Power (mW)
0
20
40
60
80
0
50
100
150
200
250
300
Pump Power, mW

Figure 9.1

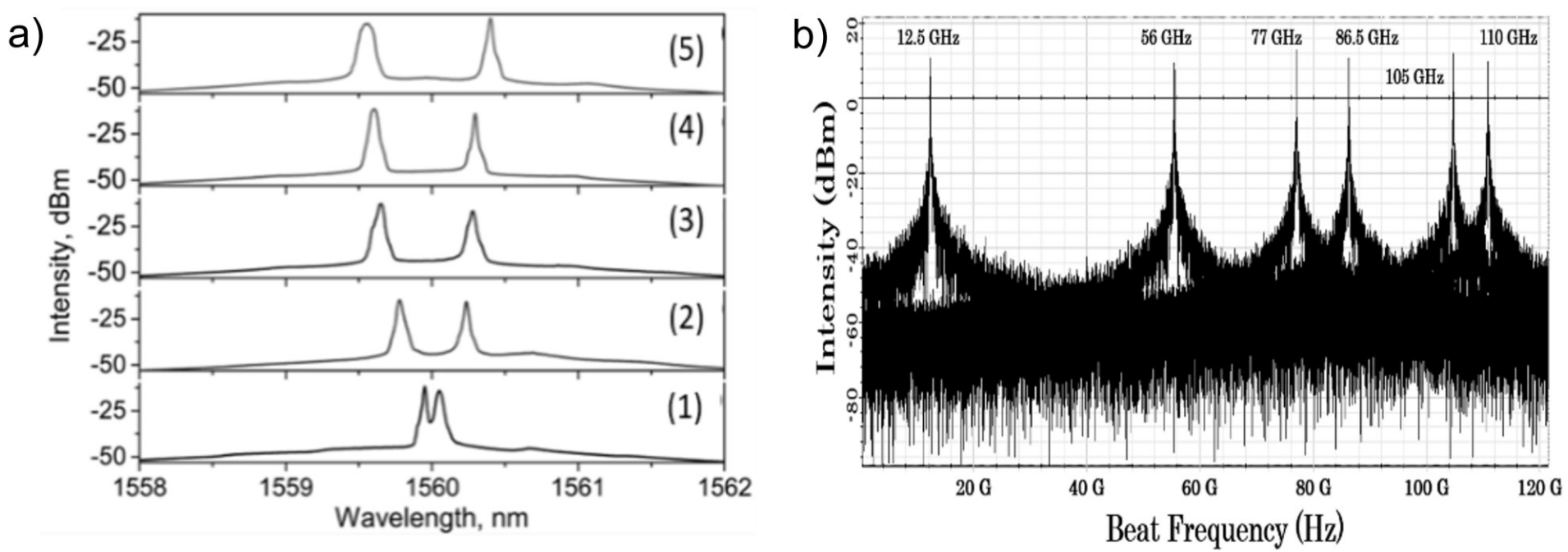
a)
(5)
(4)
(3)
(2)
(1)
-25
-50
Intensity, dBm
1558
1559
1560
1561
1562
Wavelength, nm
b)
12.5 GHz
56 GHz
77 GHz
86.5 GHz
105 GHz
110 GHz
Intensity (dBm)
20
0
-20
-40
-60
-80
20 G
40 G
60 G
80 G
100 G
120 G
Beat Frequency (Hz)

Figure 9.2

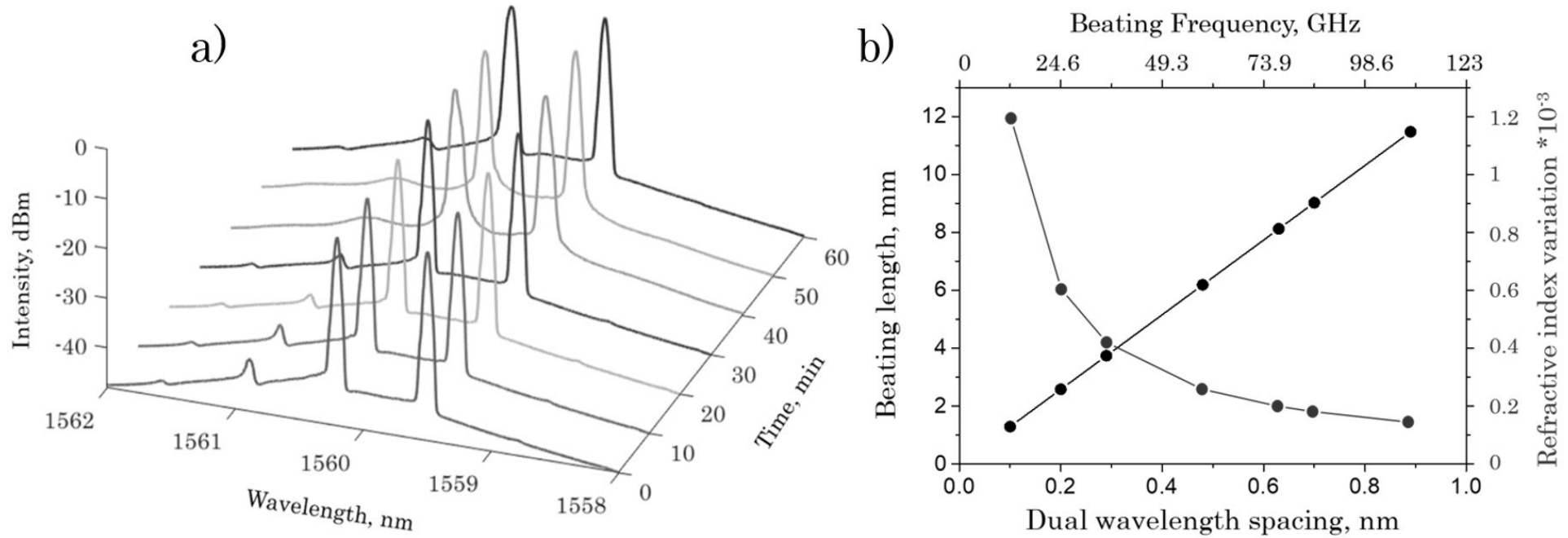
a)
Intensity, dBm
0
-10
-20
-30
-40
1562
1561
1560
1559
1558
Wavelength, nm
0
10
20
30
40
50
60
Time, min
b)
Beating Frequency, GHz
0
24.6
49.3
73.9
98.6
123
Beating length, mm
12
10
8
6
4
2
0
Refractive index variation *10-3
1.2
1
0.8
0.6
0.4
0.2
0
0.0
0.2
0.4
0.6
0.8
1.0
Dual wavelength spacing, nm

Figure 9.3

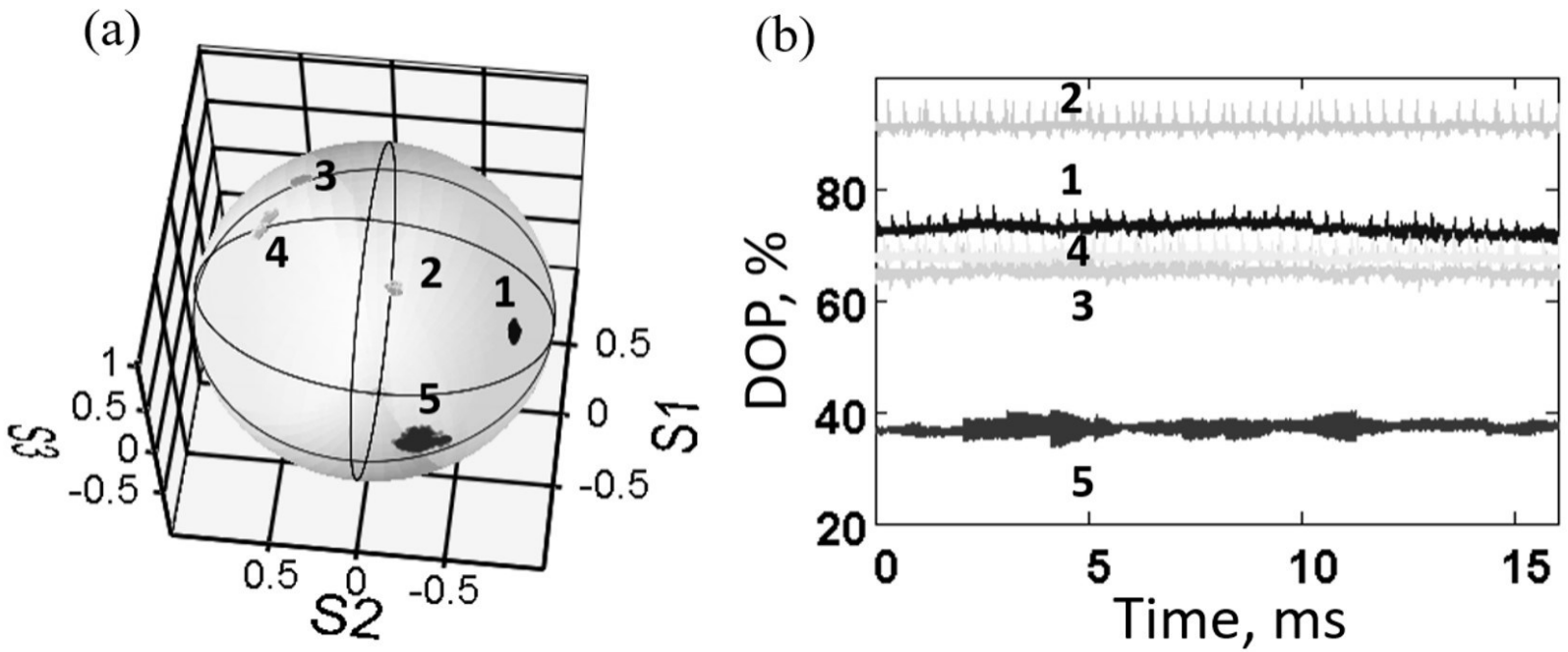
(a)
3
4
2
1
5
1
0.5
0
-0.5
S3
0.5
0
-0.5
S2
0.5
0
-0.5
S1
(b)
2
1
4
3
5
80
60
40
20
DOP, %
0
5
10
15
Time, ms

Figure 9.4

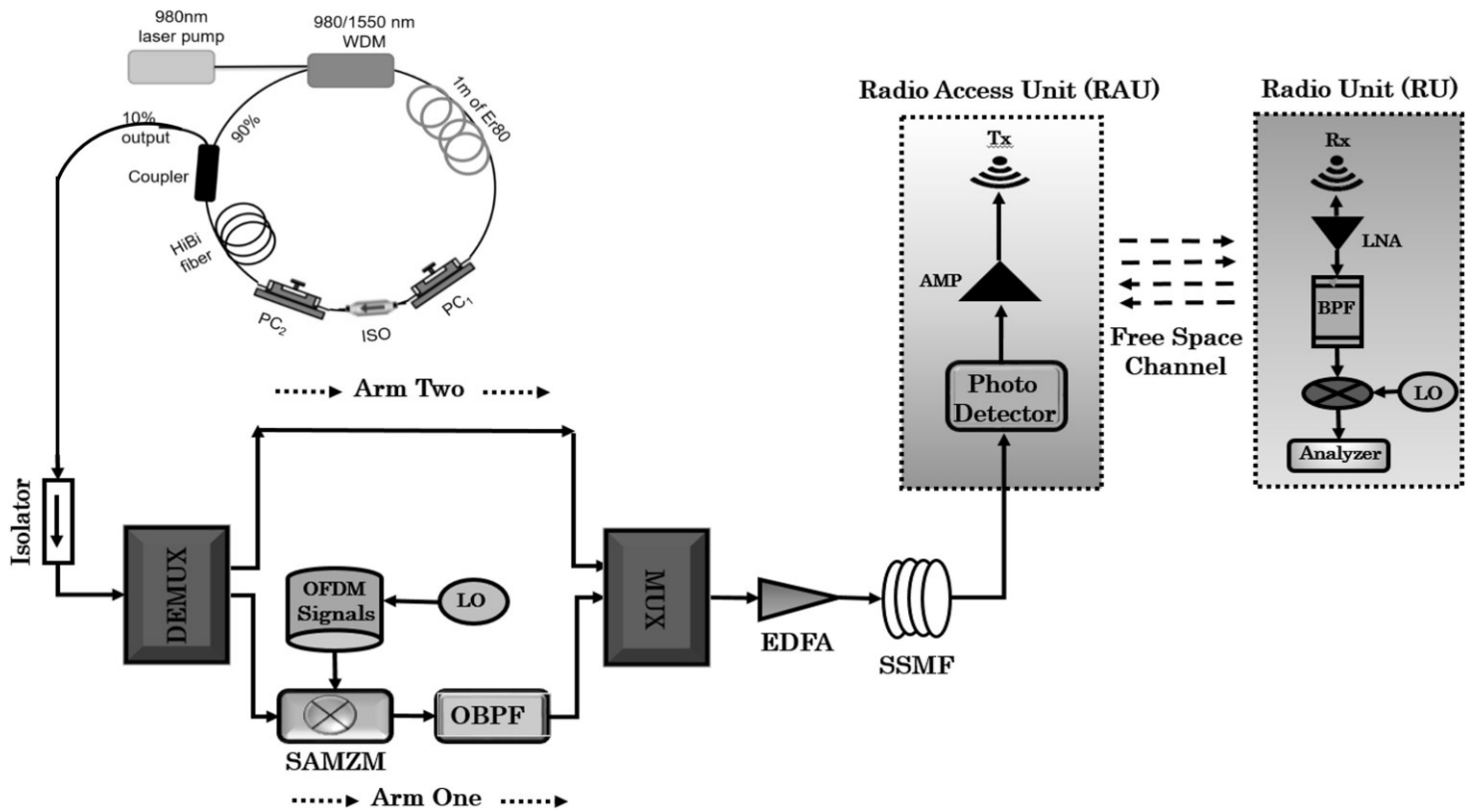
980nm
laser pump
980/1550 nm
WDM
1m of Er80
10%
output
90%
Coupler
HiBi
fiber
PC2
ISO
PC1
Arm Two
Isolator
DEMUX
OFDM
Signals
LO
MUX
EDFA
SSMF
SAMZM
OBPF
Arm One
Radio Access Unit (RAU)
Tx
AMP
Photo
Detector
Free Space
Channel
Radio Unit (RU)
Rx
LNA
BPF
LO
Analyzer

Figure 9.5

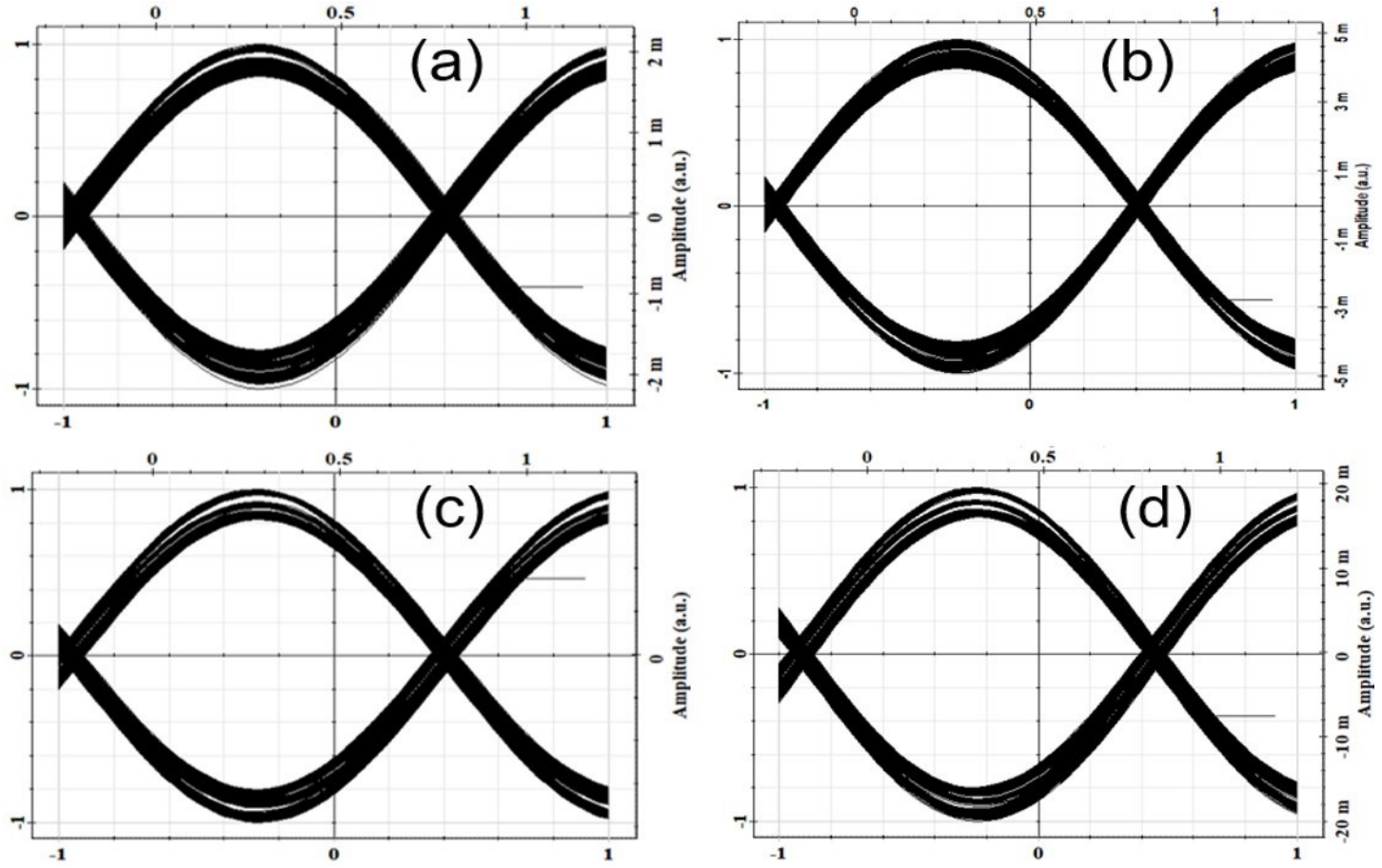

Figure 9.6

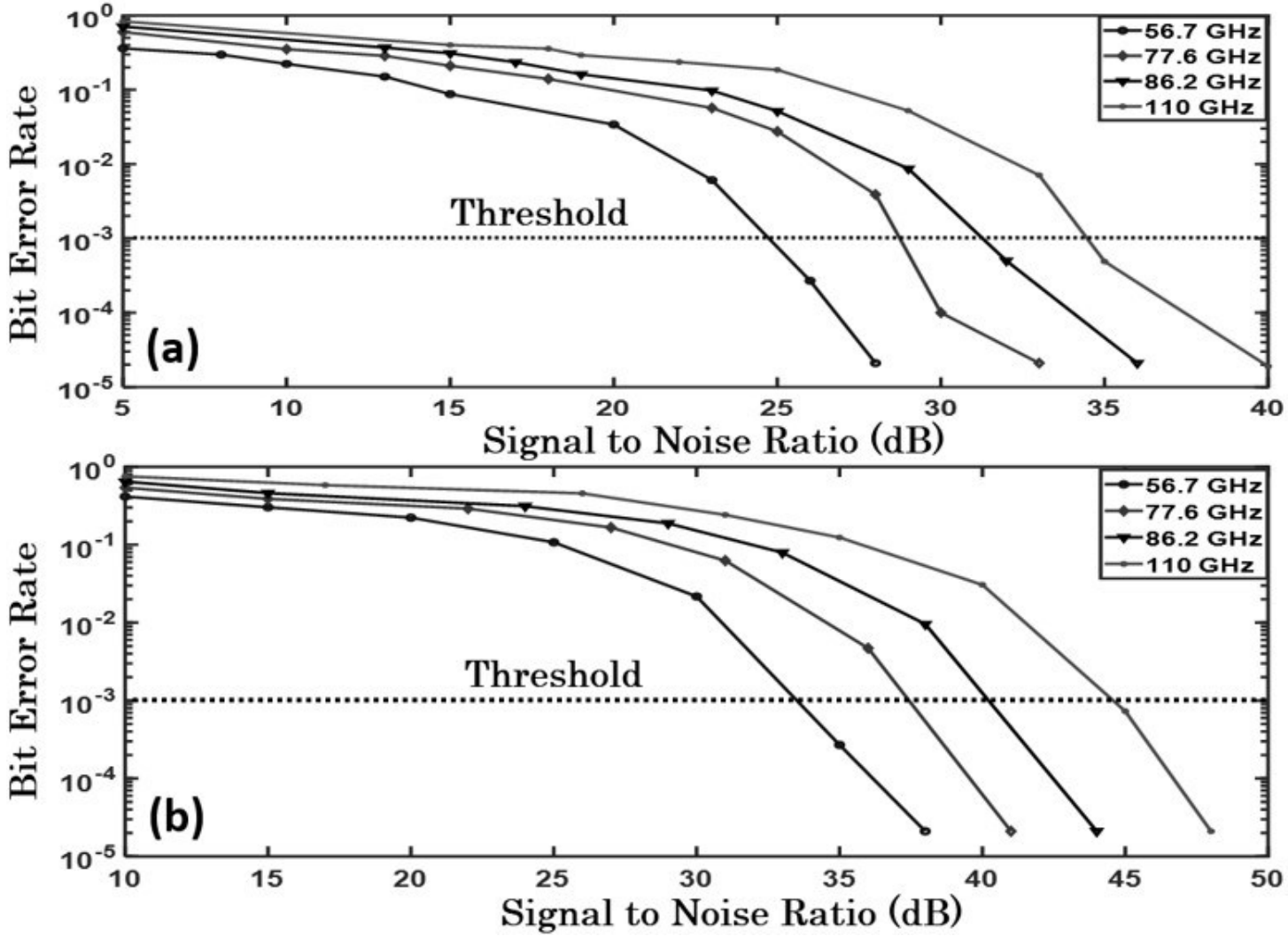
Bit Error Rate
Signal to Noise Ratio (dB)
Threshold
(a)
(b)
56.7 GHz
77.6 GHz
86.2 GHz
110 GHz

Figure 9.7

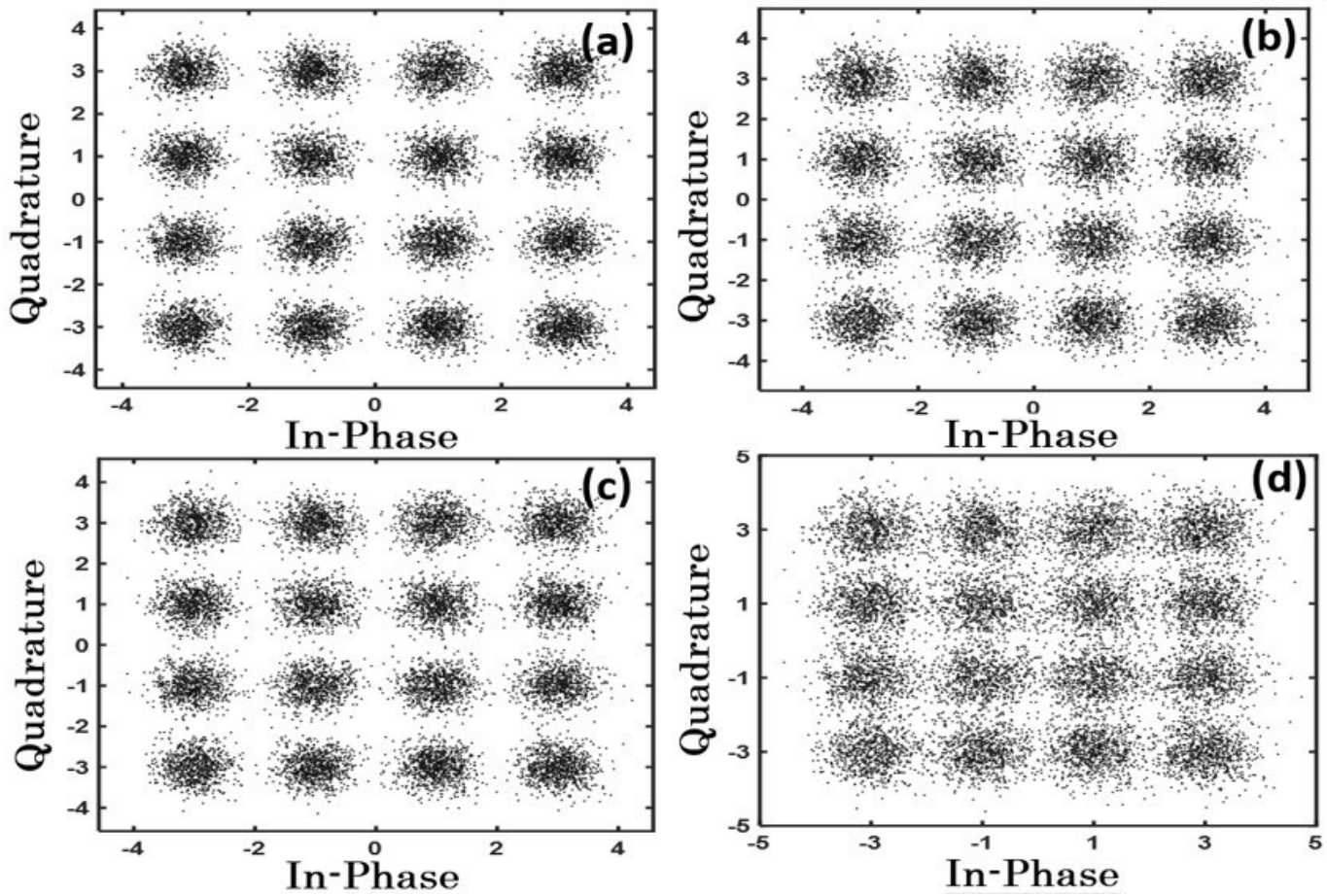

Figure 9.8

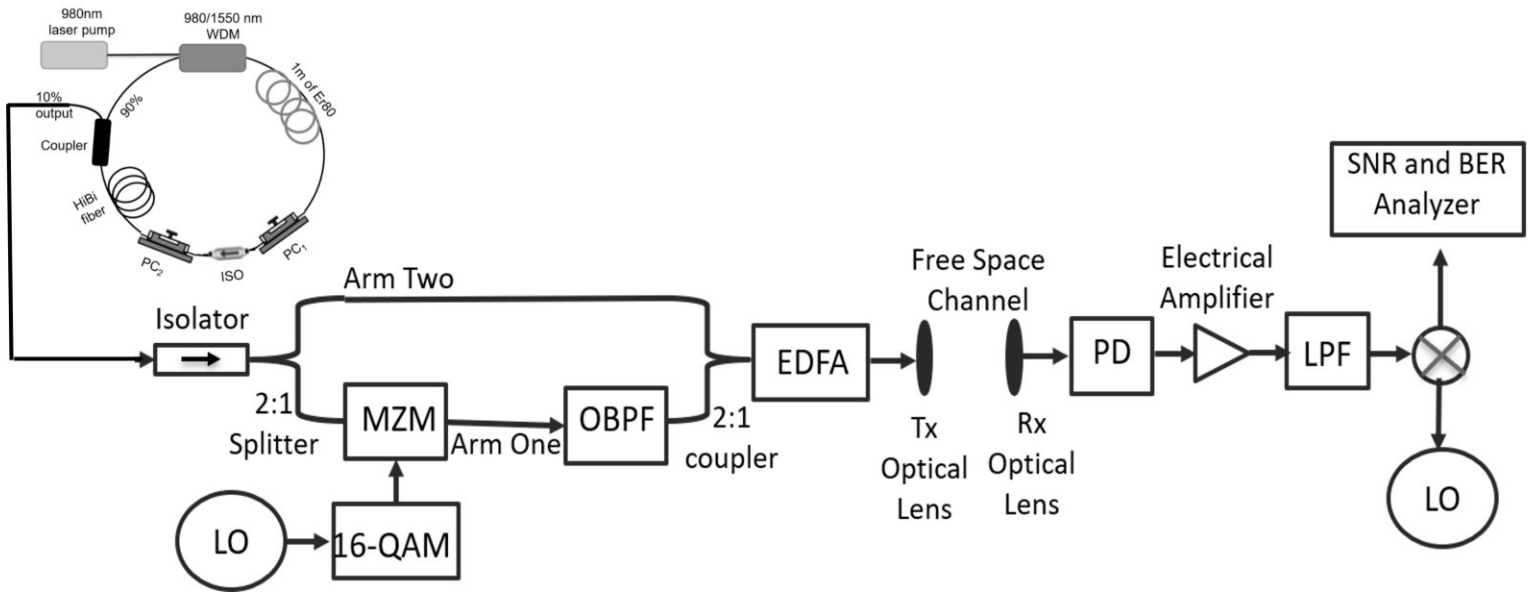
980nm
laser pump
980/1550 nm
WDM
1m of Er80
10%
output
90%
Coupler
HiBi
fiber
PC2
ISO
PC1
Isolator
Arm Two
2:1
Splitter
MZM
Arm One
OBPF
2:1
coupler
EDFA
Free Space
Channel
Tx
Optical
Lens
Rx
Optical
Lens
PD
Electrical
Amplifier
LPF
SNR and BER
Analyzer
LO
16-QAM
LO

Figure 9.9

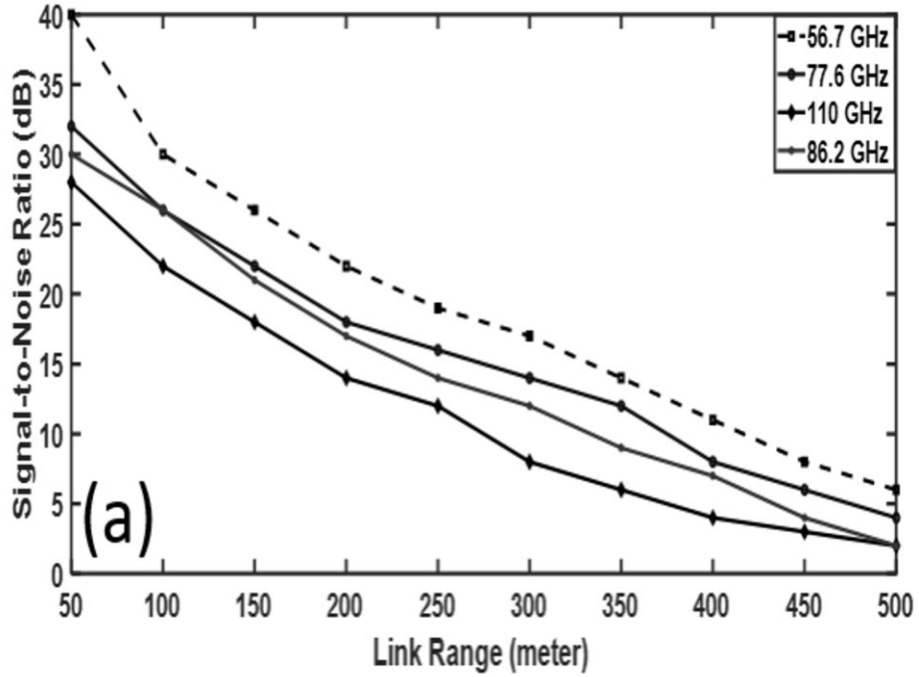
Signal-to-Noise Ratio (dB)
Link Range (meter)
56.7 GHz
77.6 GHz
110 GHz
86.2 GHz
(a)

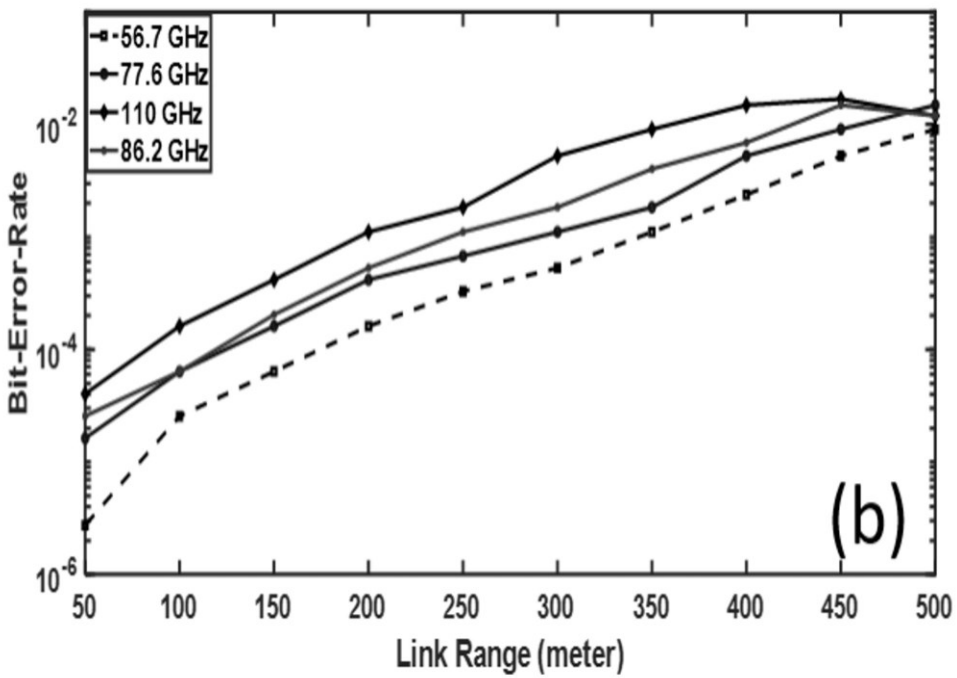
Bit-Error-Rate
Link Range (meter)
56.7 GHz
77.6 GHz
110 GHz
86.2 GHz
(b)

Figure 9.10

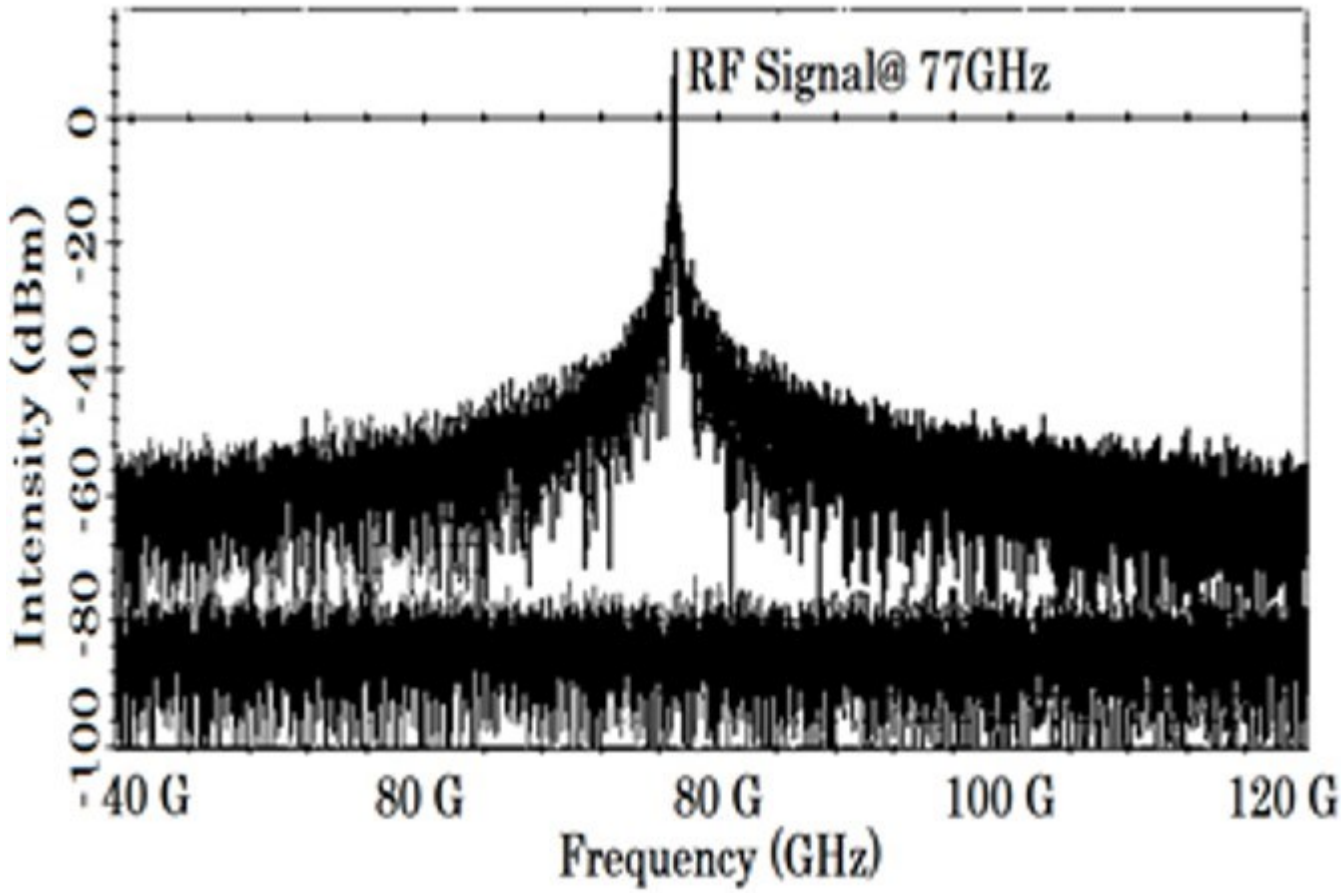
RF Signal@ 77GHz
Intensity (dBm)
0
-20
-40
-60
-80
-100
-40 G
80 G
80 G
100 G
120 G
Frequency (GHz)

Figure 9.11

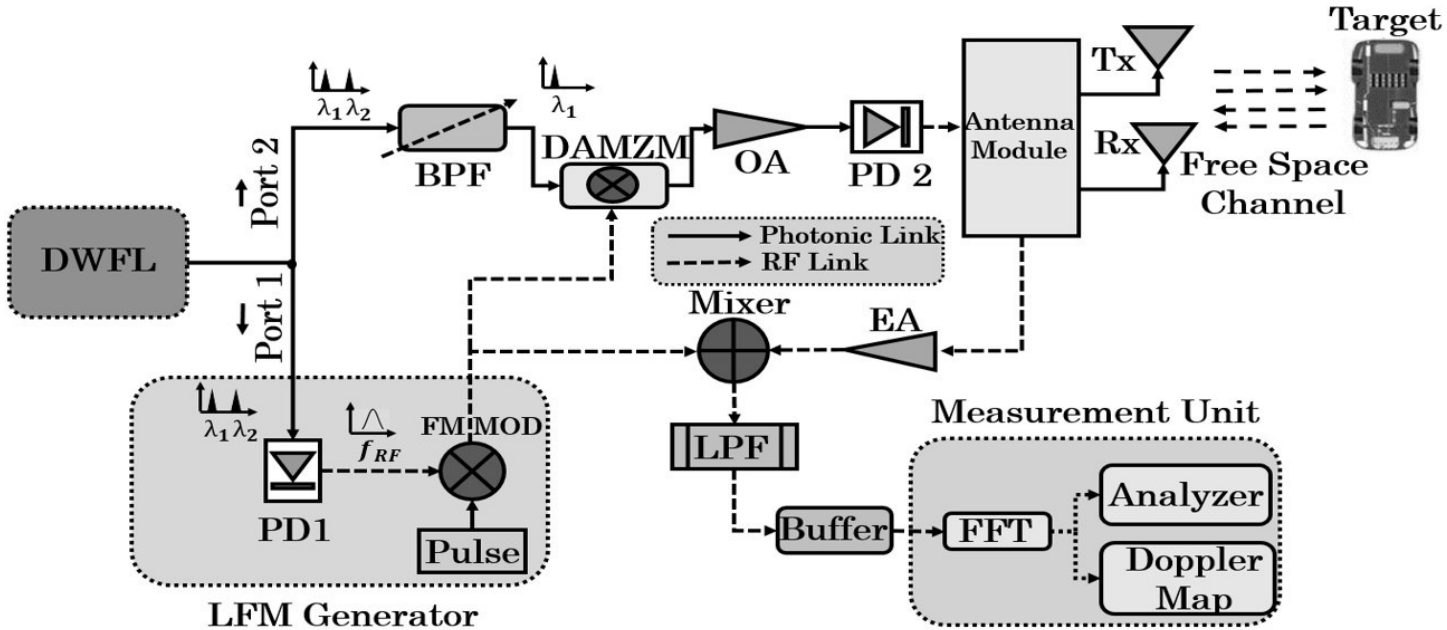
Target
Tx
Rx
Free Space Channel
Antenna Module
PD 2
OA
DAMZM
BPF
$\lambda_1\lambda_2$
λ_1
Port 2
Port 1
DWFL
Photonic Link
RF Link
Mixer
EA
$\lambda_1\lambda_2$
f_{RF}
FM MOD
PD1
Pulse
LFM Generator
LPF
Measurement Unit
Buffer
FFT
Analyzer
Doppler Map

Figure 9.12

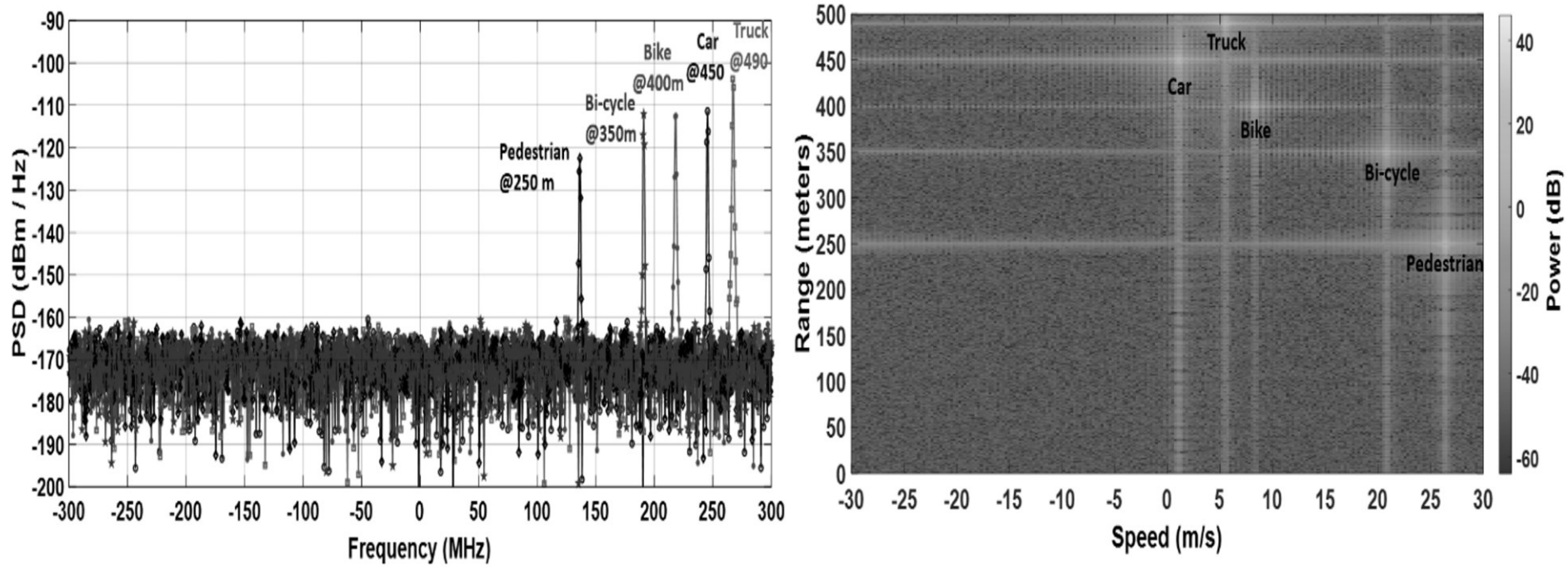
PSD (dBm / Hz)
Frequency (MHz)
Pedestrian
@250 m
Bi-cycle
@350m
Bike
@400m
Car
@450
Truck
@490
Range (meters)
Speed (m/s)
Power (dB)
Truck
Car
Bike
Bi-cycle
Pedestrian

Figure 9.13

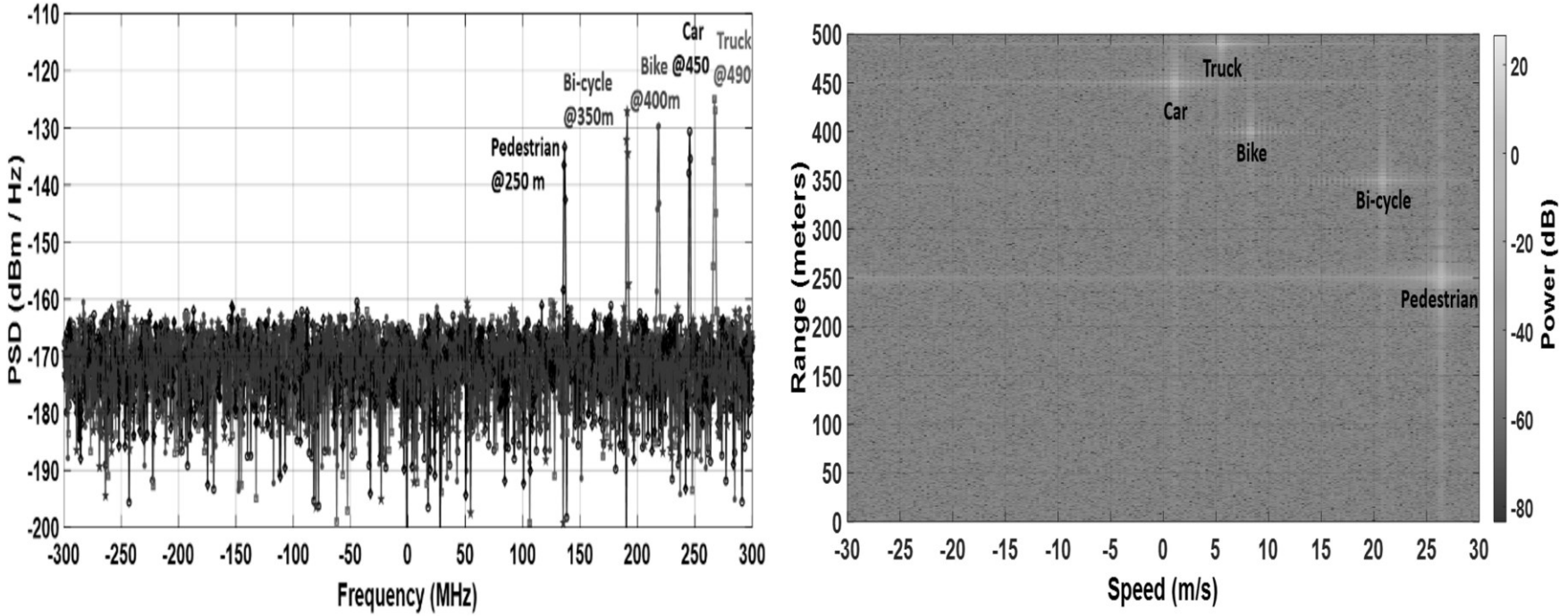
PSD (dBm / Hz)
Frequency (MHz)
Pedestrian
@250 m
Bi-cycle
@350m
@400m
Bike @450
Car
Truck
@490
Range (meters)
Speed (m/s)
Power (dB)
Truck
Car
Bike
Bi-cycle
Pedestrian

Figure 9.14